

Correlating surface stoichiometry and termination in SrTiO₃ films grown by hybrid molecular beam epitaxy

Suresh Thapa, Sydney Provence, Wencan Jin, and Ryan Comes
Physics Department, Auburn University, Auburn, AL, 36849, USA

Jason Lapano and Matthew Brahlek

Materials Science and Technology Division, Oak Ridge National Laboratory, Oak Ridge, TN, 37830, USA

Jerzy T. Sadowski

Center for Functional Nanomaterials, Brookhaven National Laboratory, Upton, NY, 11973, USA

Abstract: Hybrid oxide molecular beam epitaxy (hMBE), a thin-film deposition technique in which transition metal cations are delivered using a metal-organic precursor, has emerged as the state-of-the-art approach to the synthesis of electronic-grade complex oxide films with a stoichiometric growth window. However, numerous questions remain regarding the chemical mechanisms of the growth process and the surface properties of the resulting films. To examine these properties, thin film SrTiO₃ (STO) was prepared by hMBE using a titanium tetraisopropoxide (TTIP) precursor for Ti delivery and an elemental Sr source on annealed STO and Nb-doped STO substrates with varying TTIP:Sr flux ratios to examine the conditions for the reported stoichiometric growth window. The grown films were transferred to an appended x-ray photoelectron spectroscopy (XPS) system under ultrahigh vacuum to study the surface elemental composition in the STO samples. Low energy electron diffraction and microscopy (LEED/LEEM) measurements were also performed to correlate the XPS data with the surface termination. Also, samples were examined using x-ray diffraction (XRD) in order to compare our surface sensitive results with previously reported measurements of the bulk of the films in the literature. We find that a surface exhibiting a mixture of SrO and TiO₂ termination, or a full SrO termination is necessary to obtain stoichiometric adsorption-controlled step-flow growth. These results indicate that surface Sr is necessary to maintain chemical equilibrium. These results can open new opportunities for the study of interfacial structures synthesized via hMBE.

Introduction:

Novel properties governed by the polar discontinuity at a heterojunction have been a central focus of oxide thin film research for over a decade. The electronic reconstruction at the interface due to the polar discontinuity between oxides layer could generate high mobility two-dimensional electron gas (2DEG) [1,2]. Atomic-scale control of interfacial terminations between polar and non-polar materials has led to countless exciting emergent phenomena with potential applications. For example, studies of polar/non-polar LaFeO₃/SrTiO₃ interfaces [3–5] and the subsequent demonstration of photocatalytic behavior [6] reflects the importance of understanding interfacial structures and defects in these materials with a great deal of precision for future electronic and energy devices. In order to engineer these materials, however, careful control over the synthesis process is required, which has led to the continued improvement of epitaxial growth techniques.

The epitaxial growth of atomic scale complex oxide thin films has been driven by pulsed laser deposition (PLD) and molecular beam epitaxy (MBE) over the past 30 years. However, compared to the growth of traditional semiconductors, growth of complex oxides is challenging due to the lack of an adsorption-controlled growth window in MBE. Traditional oxide MBE employs effusion cells for each element and recipes have been developed for the growth of SrTiO₃ (STO) and other materials that typically use alternate shuttered deposition of the A-site and B-site cations, allowing for stoichiometry control down to ~1% precision [7]. Achieving more precise stoichiometric control, however, has proven challenging, which is combined with additional difficulties maintaining stable evaporation rates for low vapor pressure and refractive elements in the oxygen environments required for oxide MBE growth. Circumventing these aspects by using metal-organic precursors rather than elemental sources is a promising alternative to traditional oxide MBE. Hybrid MBE (hMBE) is a well-known technique for the implementation of mixed type sources combining elemental

effusion cells for A-site cations and metal organic precursors for transition metal B-site cations in reactive oxygen sources.

hMBE is a hybridization of chemical source MBE (a.k.a. metal-organic MBE) and reactive oxide MBE. Epitaxial growth for several refractory metal oxides, including vanadates, zirconates, and titanates, relies on hMBE [8–15]. Unexpectedly, hMBE was found to exhibit an adsorption-controlled growth window for stoichiometric STO growth when a titanium tetra-isopropoxide (TTIP) precursor was used for titanium delivery in conjunction with evaporation of Sr from a conventional effusion cell [13]. The self-regulated growth window provides an avenue to control the stoichiometry of both the cations and anions which compensates unavoidable drift in effusion cell fluxes over the course of the growth. The presence of a growth window for STO via hMBE is now well-established and has led to the highest mobility *n*-STO films on record [12,16]. STO is one of the most widely studied perovskite oxide structures in terms of bulk and surface properties due to its unique properties along with the simple cubic structure. A growth window has also been reported for several other materials, including SrVO₃ [14] and BaSnO₃ [17], yielding some of the best electronic properties reported to date in these materials. However, evaluating the presence of a growth window for STO and other complex oxides has focused primarily on bulk parameters to determine if defects are present within the material. X-ray diffraction (XRD) studies of the strong dependence of the film lattice parameters on stoichiometry have traditionally been used to evaluate the presence of a growth window [2,8–11]. Transport measurements have similarly shown high mobility and low resistivity for stoichiometric films of STO, BaSnO₃, and SrVO₃. These approaches are effective for the growth of high-quality thin films, but there have been limited studies to enable the use of hybrid MBE for interfacial phenomena in materials.

The possibility of preparing STO and other oxide films with repeatable and well-characterized surface terminations through hMBE offers a great deal of promise. To date, most heterostructures grown by hMBE have varied only the A-site cation, while maintaining chemical continuity across the B-site [20–22]. However, in multilayer structures combining dissimilar A-site and B-site cations, understanding of interfacial termination is critical to understanding functional properties [3,23,24]. At present, however, the surface of hybrid-grown STO films is poorly understood, making research on such complex heterostructures difficult to pursue. In spite of decades of studies, the stability of various STO surface terminations and reconstructions is still a matter of great debate [25–28]. In most SrTiO₃ MBE film growth, *in situ* reflection high energy electron diffraction (RHEED) has been applied to monitor the growth in real time domain, though *in-vacuo* X-ray photoelectron spectroscopy (XPS) studies have never been reported. RHEED measurements have been important for quantifying the surface reconstructions to establish a growth window, with reports that a c(4×4) surface reconstruction is indicative of the best film stoichiometry as determined through XRD and electron mobility measurements [10]. However, the actual surface termination and chemistry of hybrid-grown STO films has never been reported, which is the subject of this work.

Here we focus on characterization of the surface stoichiometry of the hMBE grown film using *in vacuo* XPS and quantifying the growth window through those XPS data. By determining the surface termination of films grown by hMBE, we will determine the relationship between surface chemistry and the previously reported XRD growth window. Possible carbon contamination in the film or on the surface is also resolved through this mechanism [11], as well as determination of water and hydrogen adsorption due to residual hydrocarbons in the growth chamber after TTIP decomposition [26]. We examine the surface of STO films grown by hMBE using *in situ* and *ex situ* surface techniques, including RHEED, XPS, and low-energy electron diffraction and microscopy (LEED/LEEM) to understand the stable surface under the unusual growth conditions present during hMBE. We show that the presence of surface SrO is crucial to the growth of stoichiometric STO and that the surface chemistry is likely to be more complex than previously imagined.

Methods:

STO thin films were grown on air annealed 10×10×0.5 mm³ (001) STO single crystal substrates (MTI Crystal) in a Mantis MBE reactor with a baseline pressure of ~10⁻⁹ Torr. Air annealing of the STO substrates in a tube furnace at 1000 °C maintains a mixed surface termination of TiO₂ and SrO because no buffered oxide

etching is employed [29]. The substrates were ultrasonically cleaned in acetone and isopropanol respectively and dried with dry nitrogen gas. All substrates were cleaned in oxygen plasma in the MBE growth chamber by ramping to the 1000 °C growth temperature over ~1 hour as measured by thermocouple [9,10]. We estimate that the setpoint is ~150-200 °C higher than substrate surface temperature due to the absence of backside substrate metallization, resulting in an STO surface temperature between 800 and 850 °C. Growth and cleaning were performed in a background pressure of $\sim 3 \times 10^{-6}$ Torr O₂ with an RF plasma source driven at 300 W to supply O atoms to increase oxidation potential at the substrate surface. The plasma was left on while the cooling the film to below 300 °C.

A series of samples was grown at differing TTIP:Sr flux ratios where the Sr flux was held fixed and the TTIP gas inlet line pressure was varied. Samples are coded numerically throughout this work by the ratio of the pressure of the TTIP in the gas injection line in mTorr to the flux of SrO measured by QCM in Å/sec. While the units of these numbers cannot be compared to the literature, they serve as a proxy for comparison to reports made by other groups using beam flux pressures [9]. We report on 5 representative samples in this work, but at least 20 additional samples have also been grown with results that are consistent with what we show here. Strontium (99.99%, Sigma-Aldrich, USA) was supplied through low temperature effusion cell. The Sr flux was calibrated using quartz crystal microbalance (QCM) under oxygen environment with measured chamber pressure of 3×10^{-6} Torr. Titanium was supplied through a gas source using a metalorganic precursor TTIP (99.999%, Sigma-Aldrich, USA) from a bubbler that was connected through the gas inlet system to the growth chamber [9]. No carrier gas was used. The growth chamber shroud walls were maintained at -30 °C via a closed loop chiller and low temperature fluid (Syltherm XLT, Dow Chemical) to reduce the background water vapor pressure from the dissociated TTIP molecules. However, the chamber pressure measured by cold cathode gauge generally increases and reaches up to $\sim 5 \times 10^{-6}$ Torr for the first 5-10 minutes during growth before stabilizing due to the dissociated and unreacted TTIP injected into the system.

In situ RHEED (Staib Instrument) was used to monitor the growth process and the quality of the film. RHEED intensity oscillations were used to estimate the growth rate, which was corroborated by measuring the spacing of the interference fringes in XRD scans to calculate the film thickness and dividing by the overall growth time. Growth rates were ~ 4.5 Å/min. Videos of the RHEED patterns were recorded and analyzed using k-means clustering and principal component analysis (PCA) codes developed at Auburn and inspired by previous work by Vasudevan et al [30]. PCA compresses the data while retaining the most statistically relevant features, producing a new dataset of orthogonal principle components and time-dependent loadings. The reduced data set is grouped into time clusters using k-means clustering, an unsupervised machine learning technique that groups the frames based on their statistical distance to the mean image of the cluster. This analysis captures any changes or transitions in the RHEED pattern at the time of occurrence in the growth. More information about this technique is available in our pending work [31].

Post-growth the samples were transferred from the MBE reactor to the PHI 5400 XPS (Al K α X-ray source) system through ultra-high vacuum (UHV) transfer line. An electron neutralizer gun was applied to compensate charging of the insulating samples. The surface stoichiometry of all grown samples was characterized by analyzing core level XPS spectra measured with base pressure of $\sim 1 \times 10^{-9}$ torr. Analysis of the XPS data was performed using CasaXPS. To properly align all core level peaks, the metallic O 1s peak was aligned to 530.0 eV. Measurements were made at 45° and 70° electron takeoff angles to vary the degree of surface sensitivity, with 45° providing a more bulk-sensitive probe of stoichiometry and 70° a more surface-sensitive. Though the probing depth of the 45° orientation for 95% of the signal is less than 5 nm which indicates these measurements are highly surface sensitive. A Malvern Panalytical X'Pert³ Diffractometer equipped with a 4-circle goniometer and using Cu K α_1 radiation line isolated with double bounce Ge (111) monochromator was used to 2θ - ω scans on the (002) reflection of the STO samples.

Further LEED/LEEM measurements were carried out in the XPEEM/LEEM endstation of the Electron Spectro-Microscopy (ESM, 21-ID-2) beamline at the National Synchrotron Light Source II [32] on STO samples grown on Nb:STO substrates. The sample was degassed at 120 °C with a pressure of 6×10^{-10} Torr for

1 hour. Subsequently, the sample was annealed in a preparation chamber at a pressure of 2×10^{-6} Torr of O_2 at 500 °C for 30 mins and cooled down in the same pressure of O_2 to room temperature to remove surface contamination. In this system, the electron-beam spot size in the LEED mode is 1.5 μm in diameter and the spatial resolution in the LEEM mode is < 10 nm [33]. The base pressure of the analysis chamber is 2×10^{-10} Torr.

Results and Discussion:

Figure 1 shows the RHEED patterns after growth and cool-down for the five samples grown on undoped STO substrates along $\langle 110 \rangle$ and $\langle 100 \rangle$ azimuth. The RHEED patterns show strong diffraction peaks and evidence of surface reconstructions in films with low TTIP:Sr flux (ratios of 740, 780, and 856) compared to films with a higher flux ratio. The strong Kikuchi lines reflect the high crystal quality of the film. Faint surface reconstructions are observed for samples 740, 780, and 856 but specific determination of the nature of the reconstruction is challenging. Films with higher TTIP:Sr flux (Figure 1(d-e)) show streaky RHEED patterns rather than intense spots indicating that the film is Ti-rich with high defect concentrations.

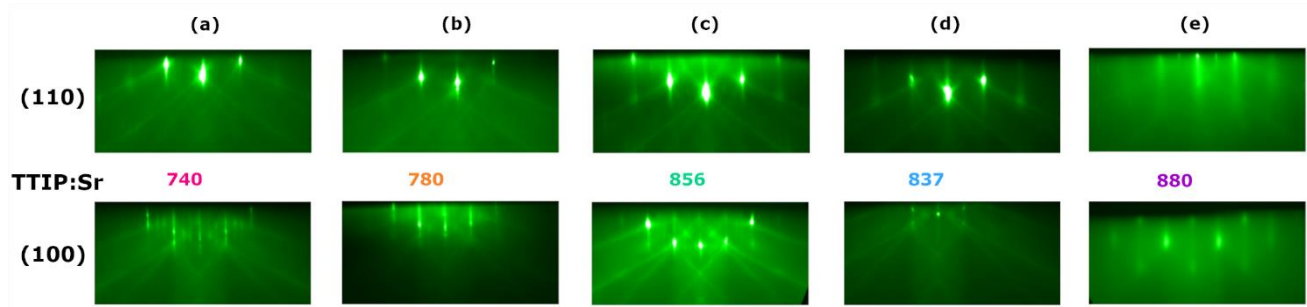


Figure 1: RHEED images (a)-(e) along 110 and 100 planes with increasing Ti:Sr peak area ratios as measured by XPS. Color-coded numbers match the samples to those in Figure 2. Calibrated flux ratios for each sample are shown in the center.

XPS measurements immediately after growth focused on quantifying Ti:Sr peak area ratios as a proxy for surface and bulk film stoichiometry. Figure 2(a) shows the normalized area ratio of Ti 2p to the Sr 3d core level as a function of TTIP:Sr flux at photoelectrons takeoff angles of 45° and 70° . The dashed dim grey and red line represent the B-site to A-site core level area ratio for air annealed STO and Nb-doped STO substrates, respectively. These references were helpful to maintain the same nominal stoichiometry and cation ratio for the STO film grown on Nb:STO substrate. With increasing TTIP:Sr flux the area ratio also increases, except for the sample with a TTIP:Sr ratio of 856. Deviation in XPS peak area ratios for the 856 sample is most likely attributable to drift or slight miscalibration in the Sr source flux. As the surface sensitivity of the XPS measurements increases, the changes in area ratio can be used to infer the primary surface termination of the sample. In fact, simply by changing the STO termination from SrO to TiO_2 , one can expect to see a significant change in the Ti 2p:Sr 3d peak area ratio of approximately 20% (see supplemental information section 1 for details).

In addition to studies of the Sr:Ti cation ratios, possible carbon contamination has also been resolved in the STO films through XPS. As the TTIP precursor contains large amounts of carbon, there have been long-standing questions as to the presence of carbon in the bulk of the film or on the surface [11]. To quantify the carbon presence, we measured the primary C 1s peak and nearby Sr 3p peak (see Supplemental Information Figure S1) [34]. The peak area was negligibly small and consistent with adsorption of carbon during the time required to transfer the sample and perform XPS measurements. Together with previous measurements [11], this suggests that hMBE samples grown with activated oxygen plasma do not have significant carbon contamination. Whether this is true for samples grown in vacuum or molecular oxygen will be determined in future work.

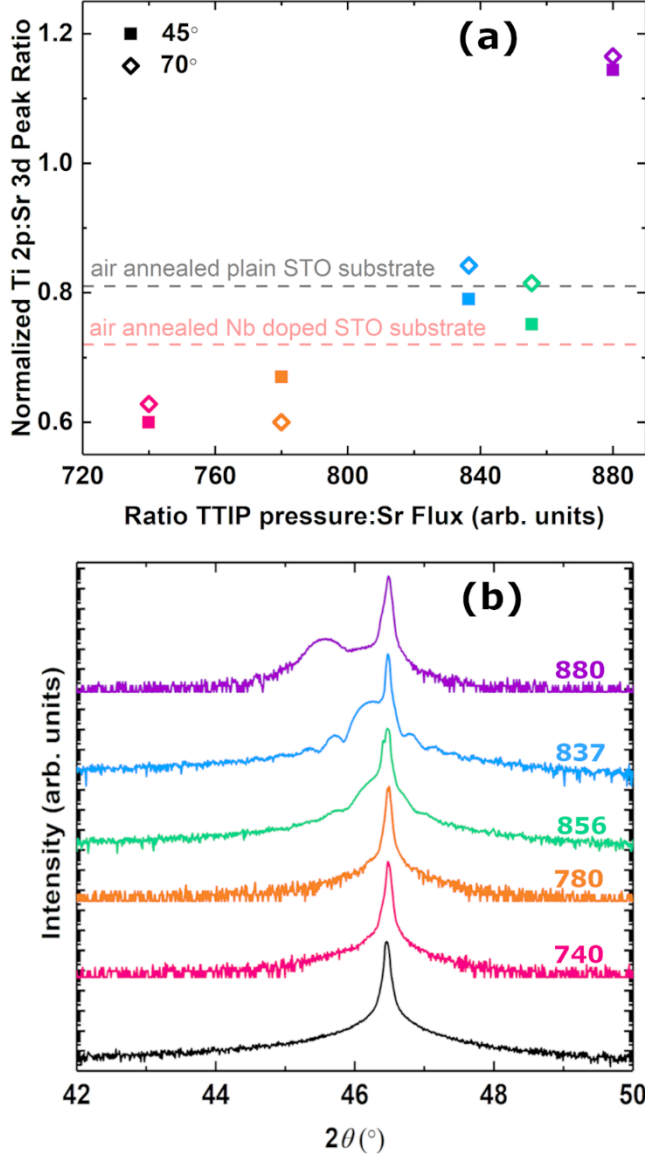


Figure 2: (a) Normalized area ratio of Ti $2p_{3/2}$ to Sr $3d_{5/2}$ as a function of TTIP pressure to Sr flux ratio at 45° and 70° x-ray incident angle in XPS. Error bars for the peak area ratios are smaller than the graphical data points. (b) Intensity as a function of 2θ in HR-XRD scans on (002) plane

A single XRD peak for a homoepitaxial film results from out-of-plane lattice matching between the substrate and film and is indicative of a stoichiometric sample with a pristine film-substrate interface with no contamination from atmospheric elements such as carbon [18]. Off-stoichiometric samples produce a secondary film peak at smaller values of 2θ consistent with a larger out-of-plane lattice parameter. In Figure 2(b), XRD scans are shown for all five films along with an air-annealed plain STO substrate (black). The 740 and 780 samples are stoichiometric whereas the 856 is slightly off-stoichiometric. The 837 and 880 samples have clear secondary peaks indicating significant off-stoichiometry in the films. The thickness fringes and shoulder at lower 2θ seen in sample 856 are most likely due to the small mismatch in lattice parameter between the film and the substrate, suggesting a slight off-stoichiometry [9].

Given the observed XPS peak areas from Figure 2(a), it seems likely that the off-stoichiometric samples (837, 856, and 880) are Ti rich and contain Sr vacancies that expand the lattice constant of the film. Conversely, samples with Ti 2p: Sr 3d area ratios less than those of the single crystal substrates (samples 740 and 780) were

found to be stoichiometric as measured by XRD. This somewhat surprising result suggests that excess Sr is present on the film surface relative to a mixed termination substrate.

With the unexpected results from the stoichiometry measurements, an understanding of the surface chemistry gives insight into the film growth process. To understand the surface chemistry of the films, the oxygen 1s (O 1s) peak for all films was further analyzed to determine the surface bonding environment. Figure 3 shows the deconvolution of the O1s core level using position constraints of 1.1 eV and 2.3 eV higher binding energy from the bulk oxygen peak for OH and surface oxygen respectively that has been applied elsewhere [35]. The two surface peaks at 1.1 and 2.3 eV have higher binding energies (531.1 eV and 532.3 eV, respectively) than the STO lattice oxygen, and are more pronounced in the 70° orientation compared to the 45° configuration due to the greater surface sensitivity provided in angle resolved XPS. Therefore, the 70° XPS measurement better quantifies the adsorbed water, hydroxyl, and undercoordinated oxygen on the surface of the film. A more pronounced 532.3 eV surface peak is observed for samples 740 and 780 (Figure 3(a-b)). The absence of the 532.3 eV surface component for films with higher TTIP:Sr flux ratio indicates that these films are primarily Ti- terminated or Ti-rich (Figure 3(c-e)).

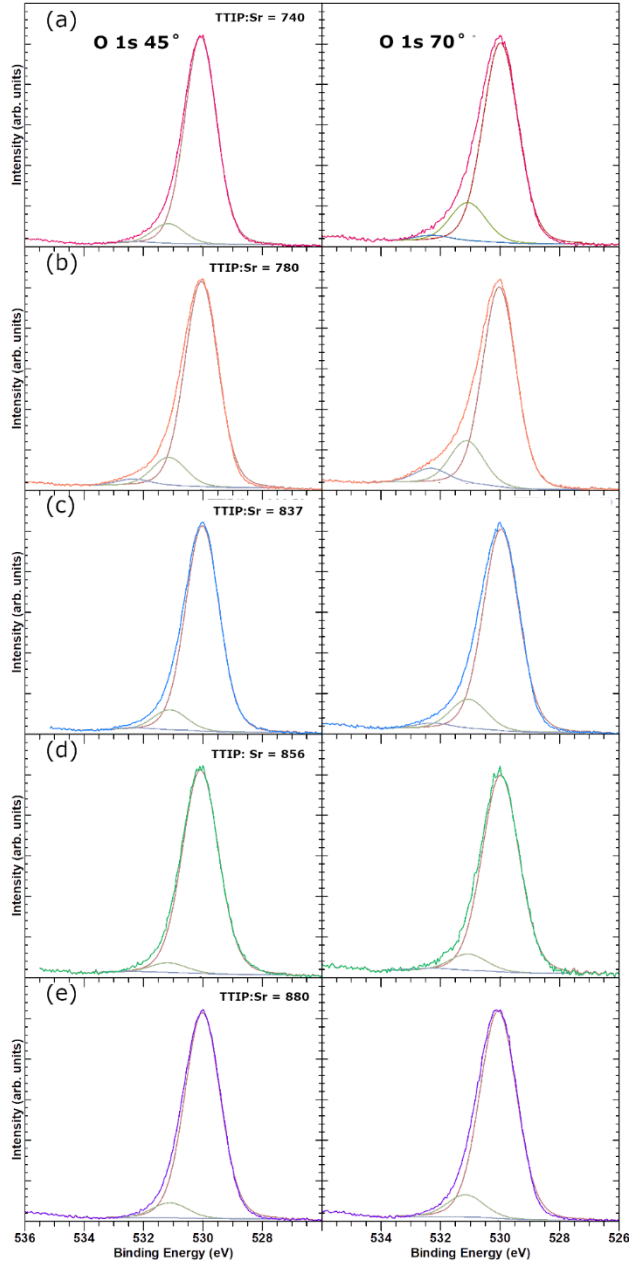


Figure 3: O 1s core level deconvolution with x-ray incident angle 45° and 70° through (a)-(e). Peaks at 530.0 eV, 531.1 eV, and 532.3 eV correspond to lattice oxygen, hydroxyl (OH), and the surface oxygen feature, respectively.

Given that sample 740 has been shown to be stoichiometric and appears to exhibit a partial SrO termination, it was chosen for further analysis of the RHEED videos to understand the growth process. PCA of the RHEED video for Sample 740 is displayed in Figure 4. By studying the time dependence of the principal components, we can glean the typical information inferred from RHEED oscillations with additional understanding of what components of the surface morphology vary with time. The first two principle components largely contain features from background noise due to cryopump vibrations and the centroid of the zeroth order RHEED streak, which are relatively uncorrelated to the film surface evolution. Conversely, oscillations with a frequency that corresponds to a growth rate of 0.45 nm/min are apparent in components 3 through 5. The features of components 3 through 5 are consistent with 2D growth modes observed previously by Vasudevan *et al* [30]. These oscillations damp out around 1100-1300 seconds and the RHEED pattern

remains uniform for the remainder of the growth. This transition is consistent with the disappearance of conventional RHEED oscillations reported by Kajdos and Stemmer for stoichiometric films [10], which was attributed to a transition to step-flow growth. Analysis of the RHEED patterns through K-means clustering (see Supplemental Information Figure S2 for more details) [34] further supports this interpretation, as the pattern for Sample 740 transitions from an initial pattern (or “cluster”) over the first ~1100 seconds to a final cluster that has minimal time variation for the remainder of the growth. Collectively, these results indicate that the film surface transforms over the first ~1100 seconds (~25 unit cells) from the poorly defined surface present on the air-annealed substrate to an equilibrium surface that undergoes step-flow growth for the remainder of the deposition.

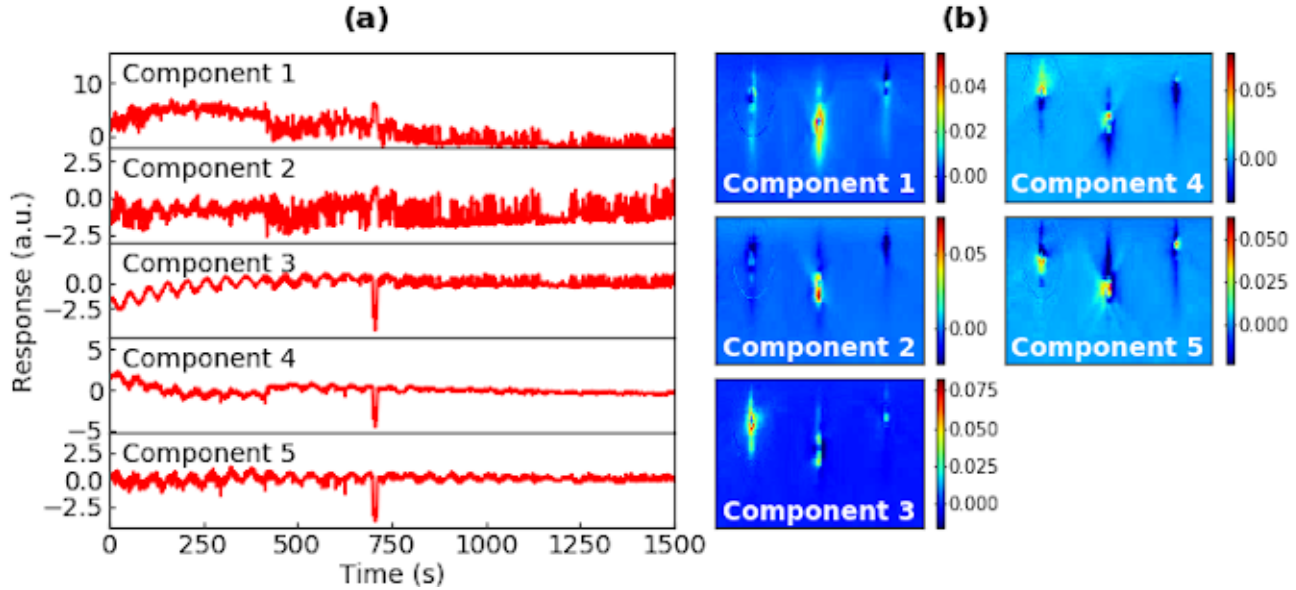


Figure 4: Time-dependent eigenvalues (left) and eigenvectors (right) for sample (a) with a constant TTIP/Sr flux ratio of 740.

To summarize the results from the homoepitaxial sample set, we find that the XRD curves in Figure 2 verify that the Sr-terminated films from XPS are stoichiometric. Meanwhile those that exhibit Ti:Sr peak area ratios comparable to or greater than what is seen in the annealed STO substrates are non-stoichiometric and presumably Ti-rich. The observed 532.3 eV O 1s peak for Sr terminated films compared to the Ti-rich samples is indicative of undercoordinated oxygen, oxygen vacancies, hydroxyl formation, or other variations in oxygen chemistry at the STO film surface. PCA of the RHEED videos for stoichiometric film (sample 740) imply uniform step flow growth of the films after ~1100 secs, which is consistent with the growth of a stoichiometric sample reported previously [9,10,13] and indicates that the film surface is in chemical equilibrium with the Sr adatom flux and TTIP and oxygen vapor. Given the relative increase in surface Sr that we observe for stoichiometric Samples 740 and 780, this suggests that the equilibrium surface for STO films grown by hybrid MBE within the growth window has a full or partial SrO termination and greater Sr concentrations at the surface than air-annealed single crystal substrates.

To further understand the apparent SrO surface termination of the samples studied thus far, an additional sample was grown with the same nominal stoichiometry and cation ratio (~0.6) from the XPS analysis as sample 740 on Nb-doped STO (see Supplemental Information Figures S3 and S4 for RHEED and XPS data respectively) [34]. LEED and LEEM measurements were performed for the STO film grown on Nb:STO to visualize the surface termination/reconstruction of the film. Figure 5 shows LEED and LEEM data for this sample. The LEED image taken with 45 eV electron energy (Figure 5(b)) clearly shows the presence of extra diffraction spots between primary spots indicating a surface reconstruction on the film surface. A $c(2 \times 2)$ reconstruction pattern is observed in Figure 5(b), as shown by the yellow circles. A faint 2×2 reconstruction

can also be seen at some energies (not shown), but was not sufficiently intense for isolation in LEEM studies. A bright field LEEM (BF-LEEM) image at 20 eV and dark field LEEM (DF-LEEM) image with $c(2\times 2)$ at 22 eV (Figure 5(c-d)) show that the reconstruction is not uniform across the whole surface. As the $c(2\times 2)$ spot was intense enough, the DF-LEEM image was reproduced using this spot and BF-LEEM image was reproduced using central bright spot. These results are consistent with a mixed surface termination, as has been observed BF-LEEM for oxide surfaces prepared by annealing [28,36]. These groups attributed the dark contrast in the BF-LEEM image to differences in the surface potential or work function for a SrO termination in comparison to a TiO_2 termination on the surface. The DF-LEEM further confirms that the dark regions in the BF-LEEM image correspond to regions with a $c(2\times 2)$ surface termination, which is commonly associated with a Sr-rich or Sr-terminated surface [10].

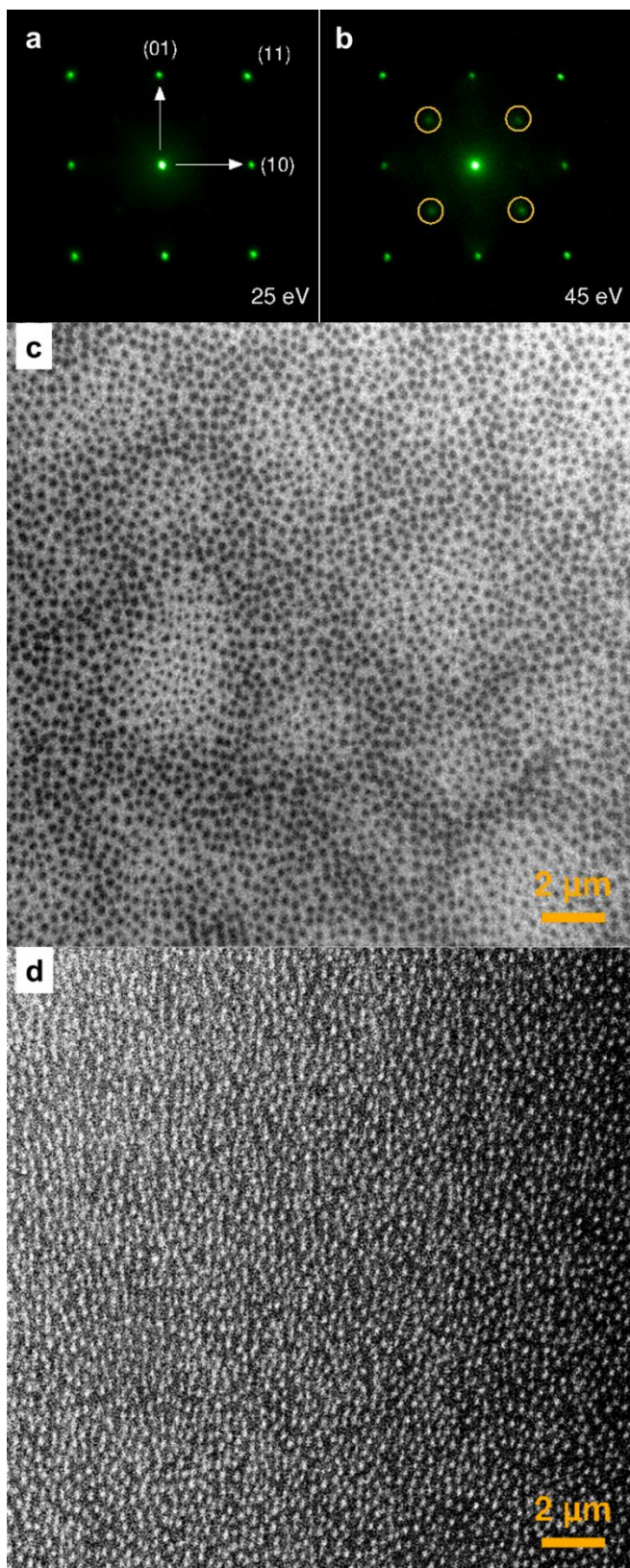


Figure 5: Low energy electron diffraction (LEED) at (a) 25 eV and (b) 40 eV electron energies, yellow circles highlight the $c(2\times 2)$ reconstructions; (c) Bright field low energy electron microscopy (LEEM) image; and (d) Dark field LEEM image highlighting the regions of $c(2\times 2)$ reconstructions.

The surface studies that we report here raise questions as to the nature of the chemical interaction during the hMBE growth process. We have shown that samples with partial SrO termination (samples 740 and 780) are stoichiometric in XRD. Conversely, the XRD results demonstrate samples with surface compositions analogous to that of an air-annealed substrate are off-stoichiometric. Surface reconstructions are observed for stoichiometric samples, although we have not observed the $c(4\times 4)$ reconstruction that others have reported [10]. Instead, a surface with partial SrO termination and evidence of a $c(2\times 2)$ surface reconstruction in some cases aligns with the ideal stoichiometry as measured by XRD. These results suggest that in order to stabilize step-flow growth in the adsorption-controlled growth regime, a significant portion of the surface must possess an SrO termination to catalyze the decomposition of TTIP. Brahlek *et al* have previously hypothesized that the TTIP sticking coefficient is greater on an SrO termination than on a TiO_2 termination, which agrees with the results we show here.

Further studies of hybrid MBE grown STO using complementary surface science techniques would enhance our understanding of surface terminations and enable the use of the technique in polar/non-polar interfaces. The existence of the extra XPS peak in the O 1s spectrum is associated with undercoordinated oxygen, oxygen vacancies, adsorbed water, or bonded OH on the surface for SrO terminations, which is not observed for TiO_2 terminated films. The presence of adsorbed water or oxygen vacancies will depend significantly on the surface termination and the ambient environment [25,26]. Given that water is a natural byproduct of the TTIP dissociation, the role of water vapor near the film surface may play a role in the chemistry of the adsorption-controlled growth. In the future, *in situ* STM, LEEM, and LEED studies of hMBE grown STO films would be extremely valuable to understand the surface structure in greater detail.

Conclusion:

In conclusion, we have demonstrated hMBE synthesis of homoepitaxial STO films with *in vacuo* XPS studies for the first time. We show that carbon contamination on the surface is negligible. We find that films exhibiting a partial or complete SrO termination are needed to produce a stoichiometric film as measured in XRD. These results are confirmed via XPS through core level Ti 2p to Sr 3d peak area ratios and the observation of O 1s surface peaks. Analysis of the RHEED pattern through PCA and K-means clustering indicate that the stoichiometric films transition to a step-flow growth regime after 20-25 unit cells. RHEED, LEEM, and LEED studies verify that surface reconstructions are associated with ideal film stoichiometry, though other complementary surface studies are needed to better probe the reconstructions and surface terminations.

Acknowledgments:

We acknowledge Z. Dai for technical assistant. ST and RBC gratefully acknowledge support from the Air Force Office of Scientific Research under award number FA9550-20-1-0034. ST, SRP, and WJ also acknowledge support from the Auburn University Department of Physics. JML and MB acknowledge support from by the U.S. Department of Energy (DOE), Office of Science, Basic Energy Sciences, Materials Sciences and Engineering Division. This research used resources of the Center for Functional Nanomaterials and National Synchrotron Light Source II, which are U.S. DOE Office of Science Facilities, at Brookhaven National Laboratory under Contract No. DE-SC0012704.

References:

- [1] A. Ohtomo and H. Y. Hwang, *Nature* **427**, 423 (2004).
- [2] S. A. Chambers, *Surface Science* **605**, 1133 (2011).
- [3] S. R. Spurgeon, P. V. Sushko, S. A. Chambers, and R. B. Comes, *Phys. Rev. Materials* **1**, 063401 (2017).

- [4] M. Nakamura, F. Kagawa, T. Tanigaki, H. S. Park, T. Matsuda, D. Shindo, Y. Tokura, and M. Kawasaki, *Phys. Rev. Lett.* **116**, 156801 (2016).
- [5] R. Comes and S. Chambers, *Physical Review Letters* **117**, 226802 (2016).
- [6] K. Nakamura, H. Mashiko, K. Yoshimatsu, and A. Ohtomo, *Applied Physics Letters* **108**, 211605 (2016).
- [7] J. H. Haeni, C. D. Theis, and D. G. Schlom, *Journal of Electroceramics* **4**, 385 (2000).
- [8] M. Brahlek, A. S. Gupta, J. Lapano, J. Roth, H.-T. Zhang, L. Zhang, R. Haislmaier, and R. Engel-Herbert, *Adv. Funct. Mater.* **28**, 1702772 (2018).
- [9] B. Jalan, R. Engel-Herbert, N. J. Wright, and S. Stemmer, *Journal of Vacuum Science and Technology A* **27**, 461 (2009).
- [10] A. P. Kajdos and S. Stemmer, *Applied Physics Letters* **105**, 191901 (2014).
- [11] B. Jalan, J. Cagnon, T. E. Mates, and S. Stemmer, *Journal of Vacuum Science & Technology A: Vacuum, Surfaces, and Films* **27**, 1365 (2009).
- [12] J. Son, P. Moetaf, B. Jalan, O. Bierwagen, N. J. Wright, R. Engel-Herbert, and S. Stemmer, *Nat Mater* **9**, 482 (2010).
- [13] B. Jalan, P. Moetaf, and S. Stemmer, *Applied Physics Letters* **95**, 032906 (2009).
- [14] M. Brahlek, L. Zhang, C. Eaton, H.-T. Zhang, and R. Engel-Herbert, *Appl. Phys. Lett.* **107**, 143108 (2015).
- [15] A. P. Kajdos, D. G. Ouellette, T. A. Cain, and S. Stemmer, *Applied Physics Letters* **103**, 082120 (2013).
- [16] B. Jalan, S. J. Allen, G. E. Beltz, P. Moetaf, and S. Stemmer, *Appl. Phys. Lett.* **98**, 132102 (2011).
- [17] A. Prakash, P. Xu, X. Wu, G. Haugstad, X. Wang, and B. Jalan, *J. Mater. Chem. C* **5**, 5730 (2017).
- [18] J. M. LeBeau, R. Engel-Herbert, B. Jalan, J. Cagnon, P. Moetaf, S. Stemmer, and G. B. Stephenson, *Applied Physics Letters* **95**, 142905 (2009).
- [19] J. Roth, E. Arriaga, M. Brahlek, J. Lapano, and R. Engel-Herbert, *Journal of Vacuum Science & Technology A* **36**, 020601 (2017).
- [20] L. R. Thoutam, J. Yue, P. Xu, and B. Jalan, *Phys. Rev. Materials* **3**, 065006 (2019).
- [21] H. Yun, J. Held, A. Prakash, T. Wang, B. Jalan, and K. A. Mkhoyan, *Microscopy and Microanalysis* **25**, 2110 (2019).
- [22] P. Moetaf, T. A. Cain, D. G. Ouellette, J. Y. Zhang, D. O. Klenov, A. Janotti, C. G. V. de Walle, S. Rajan, S. J. Allen, and S. Stemmer, *Applied Physics Letters* **99**, 232116 (2011).
- [23] S.-C. Lin, C.-T. Kuo, R. B. Comes, J. E. Rault, J.-P. Rueff, S. Nemšák, A. Taleb, J. B. Kortright, J. Meyer-Ilse, E. Gullikson, P. V. Sushko, S. R. Spurgeon, M. Gehlmann, M. E. Bowden, L. Plucinski, S. A. Chambers, and C. S. Fadley, *Phys. Rev. B* **98**, 165124 (2018).
- [24] N. Nakagawa, H. Y. Hwang, and D. A. Muller, *Nat Mater* **5**, 204 (2006).
- [25] S. A. Chambers and P. V. Sushko, *Phys. Rev. Materials* **3**, 125803 (2019).
- [26] A. E. Becerra-Toledo, J. A. Enterkin, D. M. Kienzle, and L. D. Marks, *Surface Science* **606**, 791 (2012).
- [27] M. B. S. Hesselberth, S. J. van der Molen, and J. Aarts, *Appl. Phys. Lett.* **104**, 051609 (2014).
- [28] L. Aballe, S. Matencio, M. Foerster, E. Barrena, F. Sánchez, J. Fontcuberta, and C. Ocal, *Chem. Mater.* **27**, 6198 (2015).
- [29] M. Kawasaki, K. Takahashi, T. Maeda, R. Tsuchiya, M. Shinohara, O. Ishiyama, T. Yonezawa, M. Yoshimoto, and H. Koinuma, *Science* **266**, 1540 (1994).
- [30] R. K. Vasudevan, A. Tselev, A. P. Baddorf, and S. V. Kalinin, *ACS Nano* **8**, 10899 (2014).

- [31] S. R. Provence, S. Thapa, R. Paudel, T. Truttman, P. Abhinav, B. Jalan, and R. B. Comes, Submitted for Publication. (2020).
- [32] R. M. Palomino, E. Stavitski, I. Waluyo, Y. K. Chen-Wiegart, M. Abeykoon, J. T. Sadowski, J. A. Rodriguez, A. I. Frenkel, and S. D. Senanayake, *Synchrotron Radiation News* **30**, 30 (2017).
- [33] W. Jin and R. M. Osgood, *Advances in Physics: X* **4**, 1688187 (2019).
- [34] See Supplemental Material at [URL] for details on XPS analysis, LEED/LEEM sample information, carbon XPS data, and K-means clustering analysis of RHEED.
- [35] K. A. Stoerzinger, R. Comes, S. R. Spurgeon, S. Thevuthasan, K. Ihm, E. J. Crumlin, and S. A. Chambers, *J. Phys. Chem. Lett.* **8**, 1038 (2017).
- [36] J. Jobst, L. M. Boers, C. Yin, J. Aarts, R. M. Tromp, and S. J. van der Molen, *Ultramicroscopy* **200**, 43 (2019).

Supplemental Information

S1. Ti 2p : Sr 3d peak area ratio

In order to understand how much shift in Ti 2p : Sr 3d peak area ratio could occur from experimental result if the film has completely either terminations, a simple theoretical model was created. In this model, an intensity $I(z)$ of SrO and TiO₂ layer in a STO film was calculated by assuming complete ($A_{SrO/TiO_2} = 1$) SrO and TiO₂ termination in each half a unit cell STO film depth (z) alternately up-to 5 nm. For the x-ray incident angle (θ) of 45° and wavelength (λ) 1.5 nm, all the calculated intensities are summed and evaluated the ratio of $I_{TiO_2}(z)$ to $I_{SrO}(z)$. In comparison to the STO substrate the area ratio shifts up-to ~20% depending upon the type of termination.

$$I(z) = A_{SrO/TiO_2} e^{-z/\lambda \cos \theta} \quad (1)$$

S2. Carbon contamination

Figure S1 shows the core level XPS scan for C 1s in one of the representative film with photoelectrons takeoff angle at 45°.

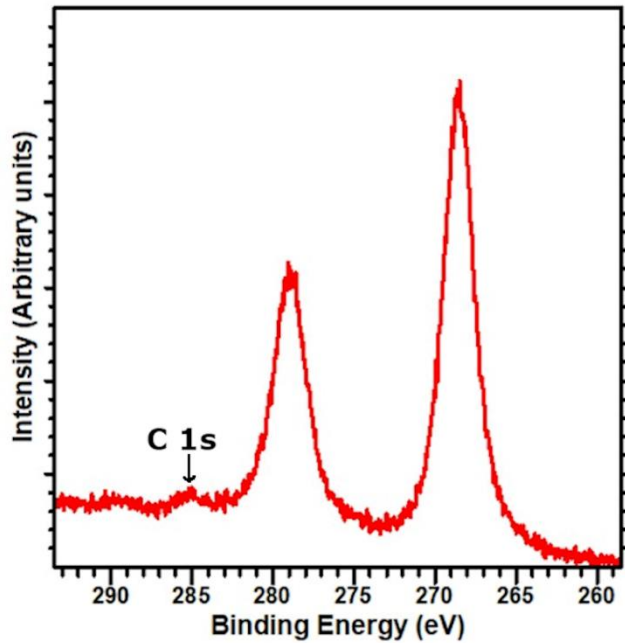


Figure S1: C1s core level with x-ray incident angle 45°.

S3. Principal Component Analysis

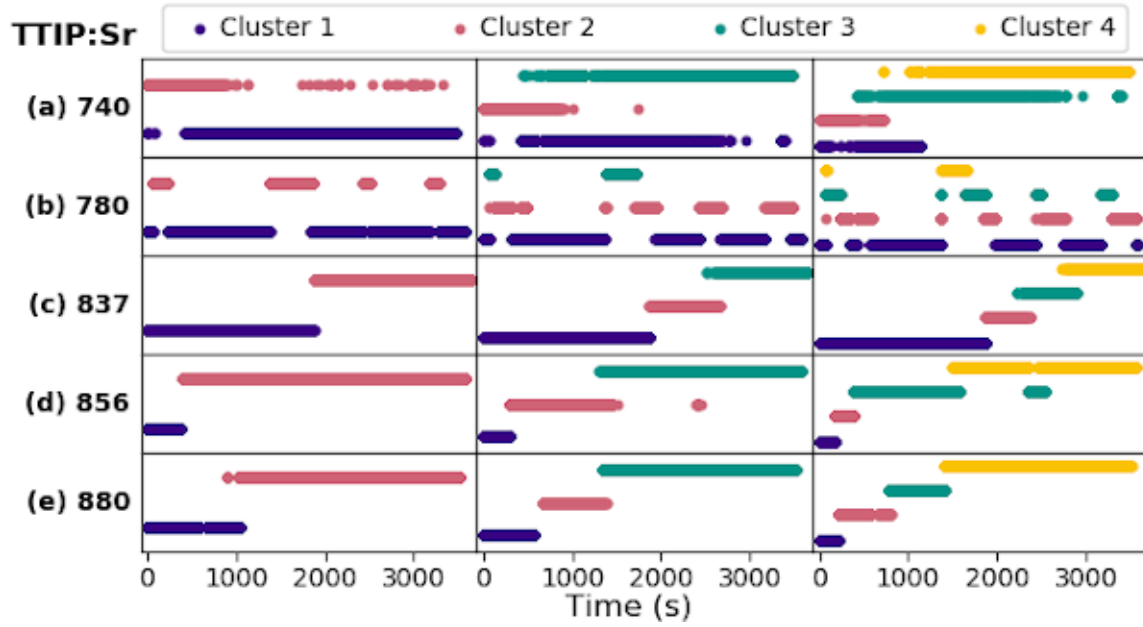


Figure S2: K-means clustering for samples (a)-(e) using 2-4 clusters.

Figure S2 shows K-means clustering for the 5 samples, with clear trends between the stoichiometric samples (740 and 780) and those that are non-stoichiometric (837, 856, and 880). The stoichiometric samples exhibit minimal changes to the RHEED pattern during growth, with the only apparent change in the clustering occurring in Sample 740 after transitioning to the step-flow growth regime. Meanwhile, the off-stoichiometric samples have abrupt changes in clustering, which suggests an accumulation of defects over the course of the growth due to excess Ti flux.

S4. RHEED and XPS data for sample 740 on Nb-doped STO

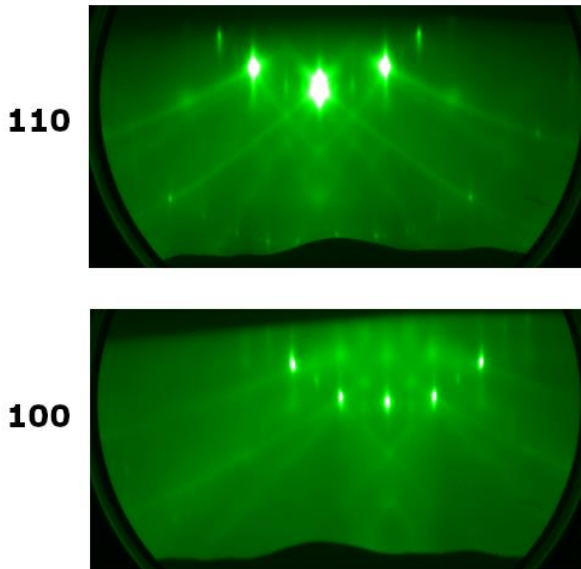


Figure S3: RHEED patterns along 110 and 100 azimuth for STO film on Nb doped STO substrate.

Figure S3 is a RHEED pattern for the sample grown on the Nb-doped STO substrate with the same nominal stoichiometry and cation ratio (~ 0.6) from the XPS analysis as Sample 740. Surface reconstructions are more visible compared to 740 sample along either azimuth. Reconstruction peaks indicate that a $c(2 \times 2)$ reconstruction and (2×2) reconstruction are present, in agreement with the observations by LEED and LEEM.

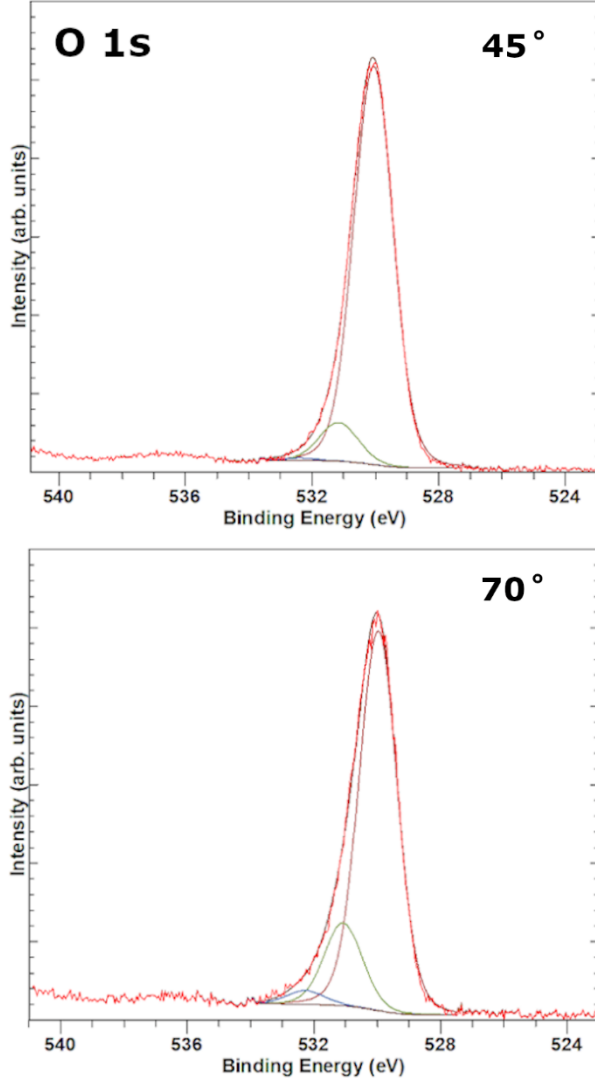


Figure S4: O1s core level with x-ray incident angle 45° and 45° for STO film on Nb doped STO substrate.

Figure S4 shows the O 1s the equivalent deconvolution with constraints as described in the main text for the LEEM/LEED sample grown with the same nominal stoichiometry and cation ratio (~ 0.6) from the XPS analysis as Sample 740 on a Nb-doped STO substrate. As with Samples 740 and 780, this deconvolution shows that the surface oxygen peak at 532.3 eV is more pronounced by relatively surface sensitive orientation of the XPS measurement. The magnitude of the surface component is nearly same as that for the 740 sample. A comparable cation area ratio along with O 1s peak deconvolution reflects same surface chemistry as 740 sample.

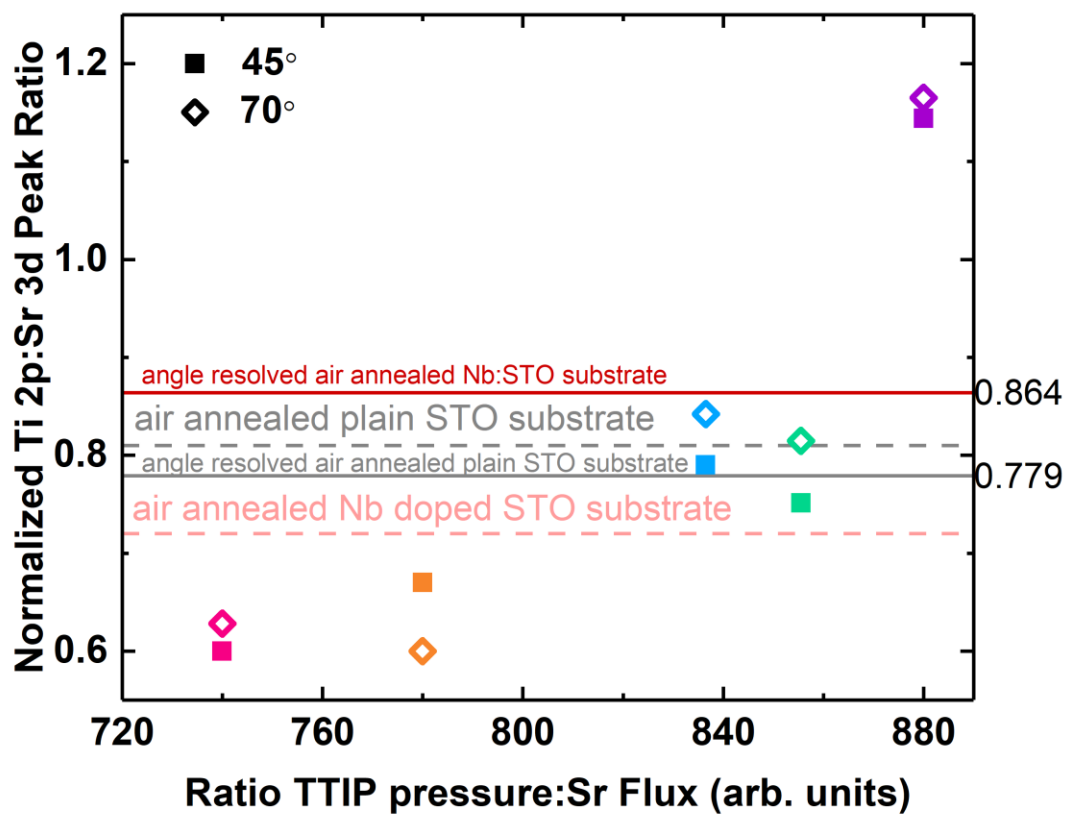


Figure S5: Replication of Figure 2a including angle-resolved data for single crystal substrates.